

1-23-2004

Measurement of the average time-integrated mixing probability of b -flavored hadrons produced at the Fermilab Tevatron

Darin Acosta

University of Florida, acosta@phys.ufl.edu

Kenneth A. Bloom

University of Nebraska-Lincoln, kbloom2@unl.edu

Collider Detector at Fermilab Collaboration

Follow this and additional works at: <http://digitalcommons.unl.edu/physicsbloom>



Part of the [Physics Commons](#)

Acosta, Darin; Bloom, Kenneth A.; and Fermilab Collaboration, Collider Detector at, "Measurement of the average time-integrated mixing probability of b -flavored hadrons produced at the Fermilab Tevatron" (2004). *Kenneth Bloom Publications*. 43.
<http://digitalcommons.unl.edu/physicsbloom/43>

This Article is brought to you for free and open access by the Research Papers in Physics and Astronomy at DigitalCommons@University of Nebraska - Lincoln. It has been accepted for inclusion in Kenneth Bloom Publications by an authorized administrator of DigitalCommons@University of Nebraska - Lincoln.

Measurement of the average time-integrated mixing probability of b -flavored hadrons produced at the Fermilab Tevatron

D. Acosta,¹⁴ T. Affolder,⁷ H. Akimoto,⁵¹ M. G. Albrow,¹³ D. Ambrose,³⁷ D. Amidei,²⁸ K. Anikeev,²⁷ J. Antos,¹ G. Apollinari,¹³ T. Arisawa,⁵¹ A. Artikov,¹¹ T. Asakawa,⁴⁹ W. Ashmanskas,² F. Azfar,³⁵ P. Azzi-Bacchetta,³⁶ N. Bacchetta,³⁶ H. Bachacou,²⁵ W. Badgett,¹³ S. Bailey,¹⁸ P. de Barbaro,⁴¹ A. Barbaro-Galtieri,²⁵ V. E. Barnes,⁴⁰ B. A. Barnett,²¹ S. Baroiant,⁵ M. Barone,¹⁵ G. Bauer,²⁷ F. Bedeschi,³⁸ S. Behari,²¹ S. Belforte,⁴⁸ W. H. Bell,¹⁷ G. Bellettini,³⁸ J. Bellinger,⁵² D. Benjamin,¹² J. Bensinger,⁴ A. Beretvas,¹³ J. Berryhill,¹⁰ A. Bhatti,⁴² M. Binkley,¹³ D. Bisello,³⁶ M. Bishai,¹³ R. E. Blair,² C. Blocker,⁴ K. Bloom,²⁸ B. Blumenfeld,²¹ S. R. Blusk,⁴¹ A. Bocci,⁴² A. Bodek,⁴¹ G. Bolla,⁴⁰ A. Bolshov,²⁷ Y. Bonushkin,⁶ D. Bortoletto,⁴⁰ J. Boudreau,³⁹ A. Brandl,³¹ C. Bromberg,²⁹ M. Brozovic,¹² E. Brubaker,²⁵ N. Bruner,³¹ J. Budagov,¹¹ H. S. Budd,⁴¹ K. Burkett,¹⁸ G. Busetto,³⁶ K. L. Byrum,² S. Cabrera,¹² P. Calafiura,²⁵ M. Campbell,²⁸ W. Carithers,²⁵ J. Carlson,²⁸ D. Carlsmith,⁵² W. Caskey,⁵ A. Castro,³ D. Cauz,⁴⁸ A. Cerri,²⁵ L. Cerrito,²⁰ A. W. Chan,¹ P. S. Chang,¹ P. T. Chang,¹ J. Chapman,²⁸ C. Chen,³⁷ Y. C. Chen,¹ M.-T. Cheng,¹ M. Chertok,⁵ G. Chiarelli,³⁸ I. Chirikov-Zorin,¹¹ G. Chlachidze,¹¹ F. Chlebana,¹³ L. Christofek,²⁰ M. L. Chu,¹ J. Y. Chung,³³ W.-H. Chung,⁵² Y. S. Chung,⁴¹ C. I. Ciobanu,³³ A. G. Clark,¹⁶ M. Coca,⁴¹ A. Connolly,²⁵ M. Convery,⁴² J. Conway,⁴⁴ M. Cordelli,¹⁵ J. Cranshaw,⁴⁶ R. Culbertson,¹³ D. Dagenhart,⁴ S. D'Auria,¹⁷ S. De Cecco,⁴³ F. DeJongh,¹³ S. Dell'Agnello,¹⁵ M. Dell'Orso,³⁸ S. Demers,⁴¹ L. Demortier,⁴² M. Deninno,³ D. De Pedis,⁴³ P. F. Derwent,¹³ T. Devlin,⁴⁴ C. Dionisi,⁴³ J. R. Dittmann,¹³ A. Dominguez,²⁵ S. Donati,³⁸ M. D'Onofrio,³⁸ T. Dorigo,³⁶ N. Eddy,²⁰ K. Einsweiler,²⁵ E. Engels, Jr.,³⁹ R. Erbacher,¹³ D. Errede,²⁰ S. Errede,²⁰ R. Eusebi,⁴¹ Q. Fan,⁴¹ S. Farrington,¹⁷ R. G. Feild,⁵³ J. P. Fernandez,⁴⁰ C. Ferretti,²⁸ R. D. Field,¹⁴ I. Fiori,³ B. Flaughner,¹³ L. R. Flores-Castillo,³⁹ G. W. Foster,¹³ M. Franklin,¹⁸ J. Freeman,¹³ J. Friedman,²⁷ Y. Fukui,²³ I. Furic,²⁷ S. Galeotti,³⁸ A. Gallas,³² M. Gallinaro,⁴² T. Gao,³⁷ M. Garcia-Sciveres,²⁵ A. F. Garfinkel,⁴⁰ P. Gatti,³⁶ C. Gay,⁵³ D. W. Gerdes,²⁸ E. Gerstein,⁹ S. Giagu,⁴³ P. Giannetti,³⁸ K. Giolo,⁴⁰ M. Giordani,⁵ P. Giromini,¹⁵ V. Glagolev,¹¹ D. Glenzinski,¹³ M. Gold,³¹ N. Goldschmidt,²⁸ J. Goldstein,¹³ G. Gomez,⁸ M. Goncharov,⁴⁵ I. Gorelov,³¹ A. T. Goshaw,¹² Y. Gotra,³⁹ K. Goulianos,⁴² C. Green,⁴⁰ A. Gresele,³ G. Grim,⁵ C. Grosso-Pilcher,¹⁰ M. Guenther,⁴⁰ G. Guillian,²⁸ J. Guimaraes da Costa,¹⁸ R. M. Haas,¹⁴ C. Haber,²⁵ S. R. Hahn,¹³ E. Halkiadakis,⁴¹ C. Hall,¹⁸ T. Handa,¹⁹ R. Handler,⁵² F. Happacher,¹⁵ K. Hara,⁴⁹ A. D. Hardman,⁴⁰ R. M. Harris,¹³ F. Hartmann,²² K. Hatakeyama,⁴² J. Hauser,⁶ J. Heinrich,³⁷ A. Heiss,²² M. Hennecke,²² M. Herndon,²¹ C. Hill,⁷ A. Hocker,⁴¹ K. D. Hoffman,¹⁰ R. Hollebeek,³⁷ L. Holloway,²⁰ S. Hou,¹ B. T. Huffman,³⁵ R. Hughes,³³ J. Huston,²⁹ J. Huth,¹⁸ H. Ikeda,⁴⁹ C. Issever,⁷ J. Incandela,⁷ G. Introzzi,³⁸ M. Iori,⁴³ A. Ivanov,⁴¹ J. Iwai,⁵¹ Y. Iwata,¹⁹ B. Iyutin,²⁷ E. James,²⁸ M. Jones,³⁷ U. Joshi,¹³ H. Kambara,¹⁶ T. Kamon,⁴⁵ T. Kaneko,⁴⁹ J. Kang,²⁸ M. Karagoz Unel,³² K. Karr,⁵⁰ S. Kartal,¹³ H. Kasha,⁵³ Y. Kato,³⁴ T. A. Keaffaber,⁴⁰ K. Kelley,²⁷ M. Kelly,²⁸ R. D. Kennedy,¹³ R. Kephart,¹³ D. Khazins,¹² T. Kikuchi,⁴⁹ B. Kilminster,⁴¹ B. J. Kim,²⁴ D. H. Kim,²⁴ H. S. Kim,²⁰ M. J. Kim,⁹ S. B. Kim,²⁴ S. H. Kim,⁴⁹ T. H. Kim,²⁷ Y. K. Kim,²⁵ M. Kirby,¹² M. Kirk,⁴ L. Kirsch,⁴ S. Klimentenko,¹⁴ P. Koehn,³³ K. Kondo,⁵¹ J. Konigsberg,¹⁴ A. Korn,²⁷ A. Korytov,¹⁴ K. Kotelnikov,³⁰ E. Kovacs,² J. Kroll,³⁷ M. Kruse,¹² V. Krutelyov,⁴⁵ S. E. Kuhlmann,² K. Kurino,¹⁹ T. Kuwabara,⁴⁹ N. Kuznetsova,¹³ A. T. Laasanen,⁴⁰ N. Lai,¹⁰ S. Lami,⁴² S. Lammel,¹³ J. Lancaster,²⁰ K. Lannon,²⁰ M. Lancaster,²⁶ R. Lander,⁵ A. Lath,⁴⁴ G. Latino,³¹ T. LeCompte,² Y. Le,²¹ J. Lee,⁴¹ S. W. Lee,⁴⁵ N. Leonardo,²⁷ S. Leone,³⁸ K. Li,⁵³ C. S. Lin,¹³ M. Lindgren,⁶ T. M. Liss,²⁰ J. B. Liu,⁴¹ T. Liu,¹³ Y. C. Liu,¹ D. O. Litvintsev,¹³ O. Lobban,⁴⁶ N. S. Lockyer,³⁷ A. Loginov,³⁰ J. Loken,³⁵ M. Loret,³⁶ D. Lucchesi,³⁶ P. Lukens,¹³ S. Lusin,⁵² L. Lyons,³⁵ J. Lys,²⁵ R. Madrak,¹⁸ K. Maeshima,¹³ P. Maksimovic,²¹ L. Malferrari,³ M. Mangano,³⁸ G. Manca,³⁵ M. Mariotti,³⁶ G. Martignon,³⁶ M. Martin,²¹ A. Martin,⁵³ V. Martin,³² M. Martínez,¹³ J. A. J. Matthews,³¹ P. Mazzanti,³ K. S. McFarland,⁴¹ P. McIntyre,⁴⁵ M. Menguzzato,³⁶ A. Menzione,³⁸ P. Merkel,¹³ C. Mesropian,⁴² A. Meyer,¹³ T. Miao,¹³ R. Miller,²⁹ J. S. Miller,²⁸ H. Minato,⁴⁹ S. Miscetti,¹⁵ M. Mishina,²³ G. Mitselmakher,¹⁴ Y. Miyazaki,³⁴ N. Moggi,³ E. Moore,³¹ R. Moore,²⁸ Y. Morita,²³ T. Moulik,⁴⁰ M. Mulhearn,²⁷ A. Mukherjee,¹³ T. Muller,²² A. Munar,³⁸ P. Murat,¹³ S. Murgia,²⁹ J. Nachtman,⁶ V. Nagaslaev,⁴⁶ S. Nahn,⁵³ H. Nakada,⁴⁹ I. Nakano,¹⁹ R. Naporá,²¹ F. Niell,²⁸ C. Nelson,¹³ T. Nelson,¹³ C. Neu,³³ M. S. Neubauer,²⁷ D. Neuberger,²² C. Newman-Holmes,¹³ C.-Y. P. Ngan,²⁷ T. Nigmanov,³⁹ H. Niu,⁴ L. Nodulman,² A. Nomerotski,¹⁴ S. H. Oh,¹² Y. D. Oh,²⁴ T. Ohmoto,¹⁹ T. Ohsugi,¹⁹ R. Oishi,⁴⁹ T. Okusawa,³⁴ J. Olsen,⁵² W. Orejudos,²⁵ C. Pagliarone,³⁸ F. Palmonari,³⁸ R. Paoletti,³⁸ V. Papadimitriou,⁴⁶ D. Partos,⁴ J. Patrick,¹³ G. Pauletta,⁴⁸ M. Paulini,⁹ T. Pauly,³⁵ C. Paus,²⁷ D. Pellett,⁵ A. Penzo,⁴⁸ L. Pescara,³⁶ T. J. Phillips,¹² G. Piacentino,³⁸ J. Piedra,⁸ K. T. Pitts,²⁰ A. Pompos,⁴⁰ L. Pondrom,⁵² G. Pope,³⁹ T. Pratt,³⁵ F. Prokoshin,¹¹ J. Proudfoot,² F. Ptohos,¹⁵ O. Pukhov,¹¹ G. Punzi,³⁸ J. Rademacker,³⁵ A. Rakitine,²⁷ F. Ratnikov,⁴⁴ H. Ray,²⁸ D. Reher,²⁵ A. Reichold,³⁵ P. Renton,³⁵ M. Rescigno,⁴³ A. Ribon,³⁶ W. Riegler,¹⁸ F. Rimondi,³ L. Ristori,³⁸ M. Riveline,⁴⁷ W. J. Robertson,¹² T. Rodrigo,⁸ S. Rolli,⁵⁰ L. Rosenson,²⁷ R. Roser,¹³ R. Rossin,³⁶ C. Rott,⁴⁰ A. Roy,⁴⁰ A. Ruiz,⁸ D. Ryan,⁵⁰ A. Safonov,⁵ R. St. Denis,¹⁷ W. K. Sakumoto,⁴¹ D. Saltzberg,⁶ C. Sanchez,³³ A. Sansoni,¹⁵ L. Santi,⁴⁸ S. Sarkar,⁴³ H. Sato,⁴⁹ P. Savard,⁴⁷ A. Savoy-Navarro,¹³ P. Schlabach,¹³ E. E. Schmidt,¹³ M. P. Schmidt,⁵³ M. Schmitt,³² L. Scodellaro,³⁶ A. Scott,⁶ A. Scribano,³⁸ A. Sedov,⁴⁰ S. Seidel,³¹ Y. Seiya,⁴⁹ A. Semenov,¹¹ F. Semeria,³ T. Shah,²⁷ M. D. Shapiro,²⁵ P. F. Shepard,³⁹ T. Shibayama,⁴⁹ M. Shimojima,⁴⁹ M. Shochet,¹⁰ A. Sidoti,³⁶ J. Siegrist,²⁵ A. Sill,⁴⁶ P. Sinervo,⁴⁷ P. Singh,²⁰ A. J. Slaughter,⁵³ K. Sliwa,⁵⁰ F. D. Snider,¹³ R. Snihur,²⁶ A. Solodsky,⁴² T. Speer,¹⁶ M. Spezziga,⁴⁶ P. Sphicas,²⁷ F. Spinella,³⁸ M. Spiropulu,¹⁰ L. Spiegel,¹³ J. Steele,⁵² A. Stefanini,³⁸ J. Strolgas,²⁰ F. Strumia,¹⁶ D. Stuart,⁷ A. Sukhanov,¹⁴ K. Sumorok,²⁷ T. Suzuki,⁴⁹ T. Takano,³⁴ R. Takashima,¹⁹

K. Takikawa,⁴⁹ P. Tamburello,¹² M. Tanaka,⁴⁹ B. Tannenbaum,⁶ M. Tecchio,²⁸ R. J. Tesarek,¹³ P. K. Teng,¹ K. Terashi,⁴² S. Tether,²⁷ J. Thom,¹³ A. S. Thompson,¹⁷ E. Thomson,³³ R. Thurman-Keup,² P. Tipton,⁴¹ S. Tkaczyk,¹³ D. Toback,⁴⁵ K. Tollefson,²⁹ D. Tonelli,³⁸ M. Tonnesmann,²⁹ H. Toyoda,³⁴ W. Trischuk,⁴⁷ J. F. de Troconiz,¹⁸ J. Tseng,²⁷ D. Tsybychev,¹⁴ N. Turini,³⁸ F. Ukegawa,⁴⁹ T. Unverhau,¹⁷ T. Vaiculiis,⁴¹ A. Varganov,²⁸ E. Vataga,³⁸ S. Vejcik III,¹³ G. Velev,¹³ G. Veramendi,²⁵ R. Vidal,¹³ I. Vila,⁸ R. Vilar,⁸ I. Volobouev,²⁵ M. von der Mey,⁶ D. Vucinic,²⁷ R. G. Wagner,² R. L. Wagner,¹³ W. Wagner,²² Z. Wan,⁴⁴ C. Wang,¹² M. J. Wang,¹ S. M. Wang,¹⁴ B. Ward,¹⁷ S. Waschke,¹⁷ T. Watanabe,⁴⁹ D. Waters,²⁶ T. Watts,⁴⁴ M. Weber,²⁵ H. Wenzel,²² B. Whitehouse,⁵⁰ A. B. Wicklund,² E. Wicklund,¹³ T. Wilkes,⁵ H. H. Williams,³⁷ P. Wilson,¹³ B. L. Winer,³³ D. Winn,²⁸ S. Wolbers,¹³ D. Wolinski,²⁸ J. Wolinski,²⁹ S. Wolinski,²⁸ M. Wolter,⁵⁰ S. Worm,⁴⁴ X. Wu,¹⁶ F. Würthwein,²⁷ J. Wyss,³⁸ U. K. Yang,¹⁰ W. Yao,²⁵ G. P. Yeh,¹³ P. Yeh,¹ K. Yi,²¹ J. Yoh,¹³ C. Yosef,²⁹ T. Yoshida,³⁴ I. Yu,²⁴ S. Yu,³⁷ Z. Yu,⁵³ J. C. Yun,¹³ L. Zanello,⁴³ A. Zanetti,⁴⁸ F. Zetti,²⁵ and S. Zucchelli³

(CDF Collaboration)

¹*Institute of Physics, Academia Sinica, Taipei, Taiwan 11529, Republic of China*

²*Argonne National Laboratory, Argonne, Illinois 60439, USA*

³*Istituto Nazionale di Fisica Nucleare, University of Bologna, I-40127 Bologna, Italy*

⁴*Brandeis University, Waltham, Massachusetts 02254, USA*

⁵*University of California at Davis, Davis, California 95616, USA*

⁶*University of California at Los Angeles, Los Angeles, California 90024, USA*

⁷*University of California at Santa Barbara, Santa Barbara, California 93106, USA*

⁸*Instituto de Fisica de Cantabria, CSIC–University of Cantabria, 39005 Santander, Spain*

⁹*Carnegie Mellon University, Pittsburgh, Pennsylvania 15213, USA*

¹⁰*Enrico Fermi Institute, University of Chicago, Chicago, Illinois 60637, USA*

¹¹*Joint Institute for Nuclear Research, RU-141980 Dubna, Russia*

¹²*Duke University, Durham, North Carolina 27708, USA*

¹³*Fermi National Accelerator Laboratory, Batavia, Illinois 60510, USA*

¹⁴*University of Florida, Gainesville, Florida 32611, USA*

¹⁵*Laboratori Nazionali di Frascati, Istituto Nazionale di Fisica Nucleare, I-00044 Frascati, Italy*

¹⁶*University of Geneva, CH-1211 Geneva 4, Switzerland*

¹⁷*Glasgow University, Glasgow G12 8QQ, United Kingdom*

¹⁸*Harvard University, Cambridge, Massachusetts 02138, USA*

¹⁹*Hiroshima University, Higashi-Hiroshima 724, Japan*

²⁰*University of Illinois, Urbana, Illinois 61801, USA*

²¹*The Johns Hopkins University, Baltimore, Maryland 21218, USA*

²²*Institut für Experimentelle Kernphysik, Universität Karlsruhe, 76128 Karlsruhe, Germany*

²³*High Energy Accelerator Research Organization (KEK), Tsukuba, Ibaraki 305, Japan*

²⁴*Center for High Energy Physics, Kyungpook National University, Taegu 702-701, Korea,*

Seoul National University, Seoul 151-742, Korea,

and SungKyunKwan University, Suwon 440-746, Korea

²⁵*Ernest Orlando Lawrence Berkeley National Laboratory, Berkeley, California 94720, USA*

²⁶*University College London, London WC1E 6BT, United Kingdom*

²⁷*Massachusetts Institute of Technology, Cambridge, Massachusetts 02139, USA*

²⁸*University of Michigan, Ann Arbor, Michigan 48109, USA*

²⁹*Michigan State University, East Lansing, Michigan 48824, USA*

³⁰*Institution for Theoretical and Experimental Physics, ITEP, Moscow 117259, Russia*

³¹*University of New Mexico, Albuquerque, New Mexico 87131, USA*

³²*Northwestern University, Evanston, Illinois 60208, USA*

³³*The Ohio State University, Columbus, Ohio 43210, USA*

³⁴*Osaka City University, Osaka 588, Japan*

³⁵*University of Oxford, Oxford OX1 3RH, United Kingdom*

³⁶*Universita di Padova, Istituto Nazionale di Fisica Nucleare, Sezione di Padova, I-35131 Padova, Italy*

³⁷*University of Pennsylvania, Philadelphia, Pennsylvania 19104, USA*

³⁸*Istituto Nazionale di Fisica Nucleare, University and Scuola Normale Superiore of Pisa, I-56100 Pisa, Italy*

³⁹*University of Pittsburgh, Pittsburgh, Pennsylvania 15260, USA*

⁴⁰*Purdue University, West Lafayette, Indiana 47907, USA*

⁴¹*University of Rochester, Rochester, New York 14627, USA*

⁴²*Rockefeller University, New York, New York 10021, USA*

⁴³*Instituto Nazionale de Fisica Nucleare, Sezione di Roma, University di Roma I, “La Sapienza,” I-00185 Roma, Italy*

⁴⁴*Rutgers University, Piscataway, New Jersey 08855, USA*

⁴⁵*Texas A&M University, College Station, Texas 77843, USA*

⁴⁶*Texas Tech University, Lubbock, Texas 79409, USA*

⁴⁷*Institute of Particle Physics, University of Toronto, Toronto, Canada M5S 1A7*

⁴⁸*Istituto Nazionale di Fisica Nucleare, University of Trieste/Udine, Italy*

⁴⁹University of Tsukuba, Tsukuba, Ibaraki 305, Japan⁵⁰Tufts University, Medford, Massachusetts 02155, USA⁵¹Waseda University, Tokyo 169, Japan⁵²University of Wisconsin, Madison, Wisconsin 53706, USA⁵³Yale University, New Haven, Connecticut 06520, USA

(Received 8 September 2003; published 23 January 2004)

We have measured the number of like-sign (LS) and opposite-sign (OS) lepton pairs arising from double semileptonic decays of b and \bar{b} hadrons, pair produced at the Fermilab Tevatron collider. The data samples were collected with the Collider Detector at Fermilab during the 1992–1995 collider run by triggering on the existence of $\mu\mu$ or $e\mu$ candidates in an event. The observed ratio of LS to OS dileptons leads to a measurement of the average time-integrated mixing probability of all produced b -flavored hadrons which decay weakly, $\bar{\chi} = 0.152 \pm 0.007$ (stat) ± 0.011 (syst), that is significantly larger than the world average $\bar{\chi} = 0.118 \pm 0.005$.

DOI: 10.1103/PhysRevD.69.012002

PACS number(s): 13.85.Qk, 13.20.Jf

I. INTRODUCTION

The time evolution of B_d^0 - \bar{B}_d^0 mixing has been accurately measured in a number of experiments, while B_s^0 - \bar{B}_s^0 mixing has not yet been observed. Time-independent measurements of B^0 mixing offer an experimentally distinct technique to extract B^0 mixing parameters. The time-integrated mixing probability is defined as $\bar{\chi} = \Gamma(B^0 \rightarrow \bar{B}^0 \rightarrow \ell^+ X) / \Gamma(B \rightarrow \ell^\pm X)$, where the numerator includes B_d^0 and B_s^0 mesons and the denominator includes all B hadrons. The average probability is then $\bar{\chi} = f_d \cdot \chi_d + f_s \cdot \chi_s$, where χ_d and f_d , and χ_s and f_s are the time-integrated mixing probability and the fraction of produced B_d^0 and B_s^0 mesons, respectively, that decay semileptonically. A measurement of $\bar{\chi}$ can be used to extract B^0 mixing information through χ_d and χ_s , or, alternatively, to extract information on the fractions of produced B_d^0 and B_s^0 mesons.

A precise measurement of the time-integrated mixing probability $\bar{\chi}$ at the Fermilab Tevatron can also provide indications for new physics through its comparison with the CERN e^+e^- collider LEP measurements and the time-dependent results from the Tevatron. For example, a recent publication [1] explores an explanation within the context of the minimal supersymmetric standard model for the long-standing discrepancy between the measured cross section for bottom-quark production at the Tevatron and the next-to-leading order (NLO) prediction. Reference [1] postulates the existence of a relatively light gluino \tilde{g} (mass ≈ 12 to 16 GeV/ c^2) that decays into a b quark and a light \tilde{b} squark (mass ≈ 2 to 5.5 GeV/ c^2). The pair production of such light gluinos provides a bottom-quark cross section comparable in magnitude to the conventional-QCD component. Since \tilde{g} is a Majorana particle, its decay yields both quark and antiquark; therefore, gluino pair production and subsequent decay to b quarks will generate bb and $\bar{b}\bar{b}$ pairs, as well as the $b\bar{b}$ final states that appear in conventional QCD production. The pair production of gluinos leads therefore to an increase of like-

sign dileptons from weak decays of b quarks.¹ This increase could be confused with an enhanced rate of B^0 - \bar{B}^0 mixing and result in a value of $\bar{\chi}$ larger than the world average 0.118 ± 0.005 [3]. Using a previous CDF result [4] [$\bar{\chi} = 0.131 \pm 0.020$ (stat) ± 0.016 (syst)], Ref. [1] estimates that the value of $\bar{\chi}$ at the Tevatron could be as large 0.17 .² The $\bar{\chi}$ measurement in Ref. [4] is based upon muon pairs corresponding to an integrated luminosity of 17.4 pb $^{-1}$. The present measurement, which makes use of a dimuon data set corresponding to an integrated luminosity of 105 pb $^{-1}$ and an $e\mu$ data set corresponding to approximately 85 pb $^{-1}$, supersedes our previous result.

In this study, the time-integrated mixing probability $\bar{\chi}$ is derived from the ratio of the observed numbers of LS and OS lepton pairs arising from $b\bar{b}$ production. At the Tevatron, dilepton events result from decays of heavy quark pairs ($b\bar{b}$ and $c\bar{c}$), the Drell-Yan process, charmonium and bottomonium decays, and decays of π and K mesons. Background to dilepton events also comes from the misidentification of π or K mesons. As in Ref. [4], we make use of the precision tracking provided by the CDF silicon microvertex detector to evaluate the fractions of leptons due to long-lived b - and c -hadron decays, and to the other background contributions.

Sections II and III describe the detector systems relevant to this analysis and the data selection, respectively. The analysis method, similar to the one used in Ref. [4], is discussed in Sec. IV. In Sec. V, we determine the contributions of the $b\bar{b}$ and $c\bar{c}$ production to OS and LS dileptons. The B^0 - \bar{B}^0 mixing result is derived in Sec. VI. Section VII presents cross checks and studies of systematics effects. Our conclusions are summarized in Sec. VIII.

¹Constraints to this scenario have been derived from other data analyses (see, for example, Ref. [2], and experimental references therein).

²Determinations of χ_d [5], based on the direct measurement of the oscillation frequency Δm_d , are not sensitive to this type of unconventional $b\bar{b}$ production; in fact, an extra source of like-sign b quarks, would reduce the amplitude of the mixing asymmetry, but would not affect the determination of Δm_d .

II. CDF DETECTOR AND TRIGGER

The CDF detector is described in detail in Ref. [6]. We review the detector components most relevant to this analysis. Inside the 1.4 T solenoid the silicon microvertex detector (SVX) [7], a vertex drift chamber (VTX), and the central tracking chamber (CTC) provide the tracking and momentum information for charged particles. The CTC is a cylindrical drift chamber containing 84 measurement layers. It covers the pseudorapidity interval $|\eta| \leq 1.1$, where $\eta = -\ln[\tan(\theta/2)]$. In CDF, θ is the polar angle measured from the proton direction, ϕ is the azimuthal angle, and r is the radius from the beam axis (z axis). The SVX consists of four layers of silicon microstrip detectors located at radii between 2.9 and 7.9 cm from the beam line and provides spatial measurements in the r - ϕ plane with a resolution of $13 \mu\text{m}$. It gives a track impact parameter³ resolution of about $(13 + 40/p_T) \mu\text{m}$, where p_T is the track momentum measured in the plane transverse to the beam axis and in GeV/ c units. The SVX extends ± 25 cm along the z axis. Since the vertex z distribution for $p\bar{p}$ collision is approximately a Gaussian function with an rms width of 30 cm, the average geometric acceptance of the SVX is about 60%. The transverse profile of the Tevatron beam is circular and has an rms spread of $\approx 30 \mu\text{m}$ in the horizontal and vertical directions. The p_T resolution of the combined CTC and SVX detectors is $\delta p_T/p_T = [(0.0066)^2 + (0.0009 (\text{GeV}/c)^{-1} \cdot p_T)^2]^{1/2}$. Electromagnetic (CEM) and hadronic (CHA) calorimeters with projective tower geometry are located outside the solenoid and cover the pseudorapidity region $|\eta| \leq 1.1$, with a segmentation of $\Delta\phi = 15^\circ$ and $\Delta\eta = 0.11$. A layer of proportional chambers (CES) is embedded near shower maximum in the CEM and provides a more precise measurement of the electromagnetic shower position. Two muon subsystems in the central rapidity region ($|\eta| \leq 0.6$) are used for muon identification: the central muon chambers (CMU), located behind the CHA calorimeter, and the central upgrade muon chambers (CMP), located behind an additional 60 cm of steel.

CDF uses a three-level trigger system. At the first two levels, decisions are made with dedicated hardware. The information available at this stage includes energy deposit in the CEM and CHA calorimeters, high- p_T tracks found in the CTC by a fast track processor, and track segments found in the muon subsystems. At the third level of the trigger, events are selected based on a version of the off-line reconstruction programs optimized for speed. The lepton selection criteria used by the 3rd level trigger are similar to those described in the next section.

A large fraction of the events used for this analysis are collected using two triggers that require two lepton candidates in an event. The first trigger requires two muon candidates; each muon candidate requires a track in the CTC, matched with track segments in the CMU system, corresponding to a particle with $p_T \geq 2.2 \text{ GeV}/c$. At least one of

the candidates is required to have track segments in both the CMU and CMP chambers. The second trigger requires an electron and a muon candidate. The E_T threshold for the electron is 5 GeV, where $E_T = E \sin \theta$, and E is the energy measured in the CEM. In addition, the trigger requires the presence of a CTC track with $p_T \geq 4.7 \text{ GeV}/c$ and the same ϕ angle of the CEM energy deposit. The muon candidate requires a CTC track with matched segments in the CMU chambers and $p_T \geq 2.7 \text{ GeV}/c$.

III. DATA SELECTION

For this analysis we select events which contain two and only two good leptons. Good muons are selected by requiring $p_T \geq 3 \text{ GeV}/c$ and a match between the CTC track extrapolated in the muon chambers and the muon segment within 3σ in the r - ϕ plane (CMU and CMP) and $\sqrt{12} \sigma$ in the r - z plane (CMU), where σ is a standard deviation including the effect of multiple scattering. In order to minimize misidentification of muons due to hadronic punch through, we require a muon segment in the CMP chambers as well as an energy deposit in the calorimeters larger than 0.1 GeV but smaller than 2 and 6 GeV in the CEM and CHA, respectively. The identification of good electrons makes use of the information from calorimeters and tracking chambers. We select electrons with $E_T \geq 5 \text{ GeV}$, and, as in previous analyses [8], we require the following: (1) the ratio of hadronic to electromagnetic energy of the cluster $E_{\text{had}}/E_{\text{em}} \leq 0.05$, (2) the ratio of cluster energy to track momentum $E/P \leq 1.5$, (3) a comparison of the lateral shower profile in the calorimeter cluster with that of test-beam electrons $L_{\text{shr}} \leq 0.2$, (4) the distance between the extrapolated track-position and the CES measurement in the r - ϕ and z views, $\Delta x \leq 1.5 \text{ cm}$, and $\Delta z \leq 3.0 \text{ cm}$, (5) a χ^2 comparison of the CES shower profile with those of test-beam electrons $\chi_{\text{strip}}^2 \leq 15$. Fiducial cuts on the electromagnetic shower position as measured in the CES, are applied to ensure that the electron candidate is away from the calorimeter boundaries and the energy is well measured. Electrons from photon conversions are removed using an algorithm based on track information [8].

To ensure accurate impact parameter measurement, each lepton track is required to be reconstructed in the SVX with hits nonshared with other tracks in at least two layers out of the possible four. We also require the impact parameter of each lepton track to be less than 0.2 cm with respect to the primary vertex.⁴ Lepton tracks are required to be within 5 cm from the primary vertex in the z direction. To reconstruct the primary event vertex, we first identify its z position using the tracks reconstructed in the VTX detector. When projected back to the beam axis, these tracks determine the longitudinal position with a precision of about 0.2 cm. The transverse position of the primary vertex is determined for each event by a weighted fit of all SVX tracks which have a z coordinate

³The impact parameter is the distance of closest approach of a track to the primary event vertex in the transverse plane.

⁴This cut removes most of the cosmic rays, since this background is distributed as a linear function of the impact parameter.

within 5 cm of the z -vertex position of the primary vertex. First, all tracks are constrained to originate from a common vertex. The position of this vertex is constrained by the transverse beam envelope described above. Tracks that have impact parameter significance $|d|/\sigma_d$, where σ_d is the estimate of the uncertainty on the impact parameter d , larger than three with respect to this vertex are removed and the fit is repeated. This procedure is iterated until all used tracks satisfy the impact parameter requirement. At least five tracks must be used in the determination of the transverse position of the primary vertex or we use the nominal beam-line position. We use this procedure to avoid having the primary vertex position biased by the presence of heavy flavor decays [8]. The primary vertex coordinates transverse to the beam direction have uncertainties in the range of 10–25 μm , depending on the number of tracks and the event topology. In the analysis, all events in which both leptons arise from the cascade (sequential) decay of a single b hadron are removed by selecting dilepton candidates with invariant mass greater than 5 GeV/c^2 .

IV. METHOD OF ANALYSIS

For leptons originating from the decay of long lived particles the impact parameter is $d = |\beta\gamma ct \sin(\delta)|$, where t is the proper decay time of the parent particle from which the lepton track originates, δ is the decay angle of the lepton track with respect to the direction of the parent particle, and $\beta\gamma$ is a Lorentz boost factor. The impact parameter of the lepton is proportional to the lifetime of the parent particle. The markedly different impact parameter distributions for leptons from b decays, c decays, and other sources allow the determination of the parent fractions.

The method used to determine the $b\bar{b}$ and $c\bar{c}$ content of the data has been pioneered in Ref. [4]. The procedure is to fit the observed impact parameter distribution of the lepton pairs with the expected impact parameter distributions of leptons from various sources. After data selection, the main sources of reconstructed leptons are semileptonic decays of bottom and charmed hadrons, and prompt decays of onia and Drell-Yan production.

Monte Carlo simulations are used to model the impact parameter distributions for leptons from b and c decays. We use the HERWIG Monte Carlo generator program [9] to generate hadrons with heavy flavors,⁵ the QQ Monte Carlo program [10] to decay hadrons with heavy flavor, and the QFL Monte Carlo simulation of CDF [8] to model the detector's response. Impact parameter distributions for simulated b and c decays are shown in Figs. 1(a) and 1(b), respectively. Since

⁵We use option 1500 of version 5.6, generic $2 \rightarrow 2$ hard scattering with $p_T \geq 5 \text{ GeV}/c$, with the same setting of the HERWIG parameters used in Ref. [8]. In the generic hard parton scattering, $b\bar{b}$ and $c\bar{c}$ pairs are generated by HERWIG through processes of order α_s^2 (LO) such as $gg \rightarrow b\bar{b}$ (direct production). Processes of order α_s^3 are implemented in HERWIG through flavor excitation processes, such as $gb \rightarrow gb$, or gluon splitting, in which the process $gg \rightarrow gg$ is followed by $g \rightarrow b\bar{b}$.

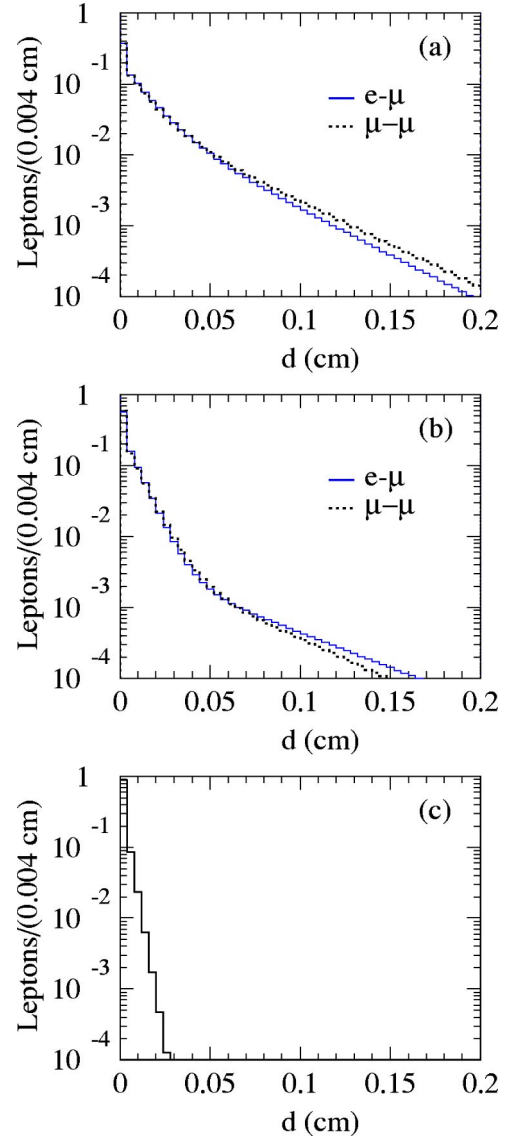


FIG. 1. Impact parameter distributions of leptons coming from b decays (a), c decays (b), and prompt leptons (c). Distributions are normalized to unit area; differences between $\mu-\mu$ and $e-\mu$ templates are due to the different p_T thresholds. The ratio of the number of events with $d \leq 0.008 \text{ cm}$ to that with $d \geq 0.008 \text{ cm}$ is 1.04, 2.85, and 32.3 for the histograms (a), (b), and (c), respectively.

lifetimes of bottom and charmed hadrons ($c\tau_B \approx 480 \mu\text{m}$ and $c\tau_D \approx 200 \mu\text{m}$) are much larger than the average SVX impact parameter resolution in these data sets ($\approx 15 \mu\text{m}$), the dominant factor determining the impact parameter distribution is the kinematics of the semileptonic decays which is well modeled by the simulation (see Sec. VII). The fraction of leptons from sequential b decays ($b \rightarrow cX, c \rightarrow lY$) is also determined with the simulation. Leptons from sequential b decays have slightly different kinematics and slightly larger ct than leptons coming from direct b decays; these two effects compensate and the simulated impact parameter distribution of leptons from sequential decays is indistinguishable from that of leptons from direct b decays. The impact parameter distribution of leptons from prompt sources such as

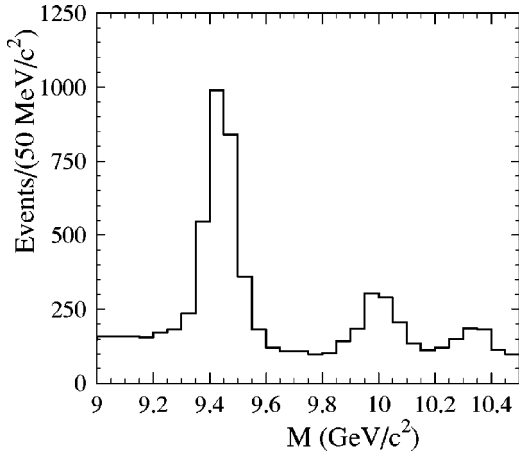


FIG. 2. Invariant mass distribution of OS dimuons in the Y region. The impact parameter distribution in Fig. 1(c) is derived using muons with invariant mass between 9.28 and 9.6 GeV/c^2 . The background is removed using dimuons with invariant mass between 9.04 and 9.2 GeV/c^2 and between 9.64 and 9.8 GeV/c^2 . Dimuon events in the mass range 9.2–10.5 GeV/c^2 , which are dominated by Y production, are not used in the $\bar{\chi}$ analysis.

quarkonia decays and Drell-Yan production is plotted in Fig. 1(c) and is derived using muons from $Y(1S)$ decays⁶ (see Fig. 2).

Lepton tracks from π and K in-flight decays are also regarded as prompt tracks since the track reconstruction algorithm rejects tracks with appreciable kinks. Tracks of π and K mesons, which mimic the lepton signal, are also regarded as prompt since the average heavy flavor contribution per event is negligible (see Sec. VII).

Since there are two leptons in an event, the fit is performed in the two-dimensional space of impact parameters. Each axis represents the impact parameter of one of the two leptons. In filling the histograms, the lepton ordering by flavor type or transverse momentum is randomized. The two-dimensional impact parameter technique exploits the fact that the lepton impact parameters are independent uncorrelated variables.⁷ The two-dimensional template distributions for each type of event are made by combining the relevant one-dimensional distributions in Fig. 1.

A binned maximum log likelihood method is used to fit simultaneously the impact parameter distributions of OS and LS dileptons. The likelihood L is defined as

$$L = \prod_i \prod_j [l_{ij}^{n(i,j)} e^{-l_{ij}/n(i,j)!}],$$

⁶We use templates derived from the data to account properly for non-Gaussian tails of the impact parameter distribution. The impact parameter distribution of electrons from a smaller statistics sample of $Z \rightarrow e^+e^-$ is also well modeled by the muon template.

⁷The correlation between the two impact parameters $\rho = \iint (d_1 - \langle d_1 \rangle)(d_2 - \langle d_2 \rangle) \delta d_1 \delta d_2 / \sigma_{d_1} \sigma_{d_2}$, is approximately 0.04 in the data samples and their heavy flavor simulations.

where $n(i,j)$ is the number of events in the (i,j) th bin. The function l_{ij} is defined as

$$l_{ij} = BB \cdot S_b(i) \cdot S_b(j) + CC \cdot S_c(i) \cdot S_c(j) + PP \cdot S_p(i) \cdot S_p(j) \\ + 0.5 \cdot \{BP \cdot [S_b(i) \cdot S_p(j) + S_p(i) \cdot S_b(j)] \\ + CP \cdot [S_c(i) \cdot S_p(j) + S_p(i) \cdot S_c(j)]\},$$

where S_b , S_c , and S_p are the impact parameter templates shown in Figs. 1(a), 1(b), and 1(c), respectively. The fit parameters BB , CC , and PP represent the $b\bar{b}$, $c\bar{c}$ and prompt dilepton contributions, respectively. The fit parameter BP (CP) estimates the number of events in which there is only one b (c) quark in the detector acceptance and the second lepton is produced by the decay or the misidentification of π and K mesons.⁸ Figure 3 compares projections of the two-dimensional distributions for each type of dilepton contribution to the likelihood. Because of sequential decay and mixing, the $b\bar{b}$ production results in both OS and LS dileptons. For LS dileptons, one expects no contribution from $c\bar{c}$ production.

We do not fit dimuon events with invariant mass between 9.2 and 10.5 GeV/c^2 since OS dimuons are dominated by Y meson production. The PP contribution to $e\mu$ events can only arise from misidentified leptons ($\tau\tau$ Drell-Yan production is negligible) and is expected to be equal for OS and SS dileptons. Therefore, in the fit to $e\mu$ data, the PP components in OS and LS dileptons are constrained to be equal within the statistical error [technically, we add the term $0.5[PP(OS) - PP(LS)]^2/[PP(OS) + PP(LS)]$ to the function $-\ln L$ used by the fit]. In dimuon events, where the Drell-Yan contribution is relevant, OS leptons have a larger PP component than LS dileptons. The BP and CP contributions, in which one lepton is fake, are expected to be the same for OS and LS dileptons, and in the fit are constrained to be equal within the statistical error. One also expects the BP and CP contributions to have approximately the same size.⁹

⁸According to the simulation, supported by the measurement in Ref. [11], approximately 90% of the $b\bar{b}$ and $c\bar{c}$ events with an identified lepton from heavy flavor decay do not contain the second heavy flavored hadron in the detector acceptance. Therefore, we ignore the small contribution to misidentified leptons due to π and K mesons from heavy flavor decays (see Sec. VII).

⁹According to the simulation, the cross section for producing at least one c hadron in the detector acceptance is approximately a factor of two larger than the cross section for producing at least one b hadron in the detector acceptance. Since the efficiency for detecting a lepton from a c decay is approximately 40% of that for detecting a lepton from a b decay, one expects the $b\bar{b}$ and $c\bar{c}$ contributions to events with at least one identified lepton to be approximately equal. In contrast, the $b\bar{b}$ and $c\bar{c}$ cross sections for producing events which contain 2 hadrons with heavy flavor in the detector acceptance are dominated by the LO term and are approximately equal; one therefore expects the $b\bar{b}$ contribution to dilepton events to be much larger than the $c\bar{c}$ contribution.

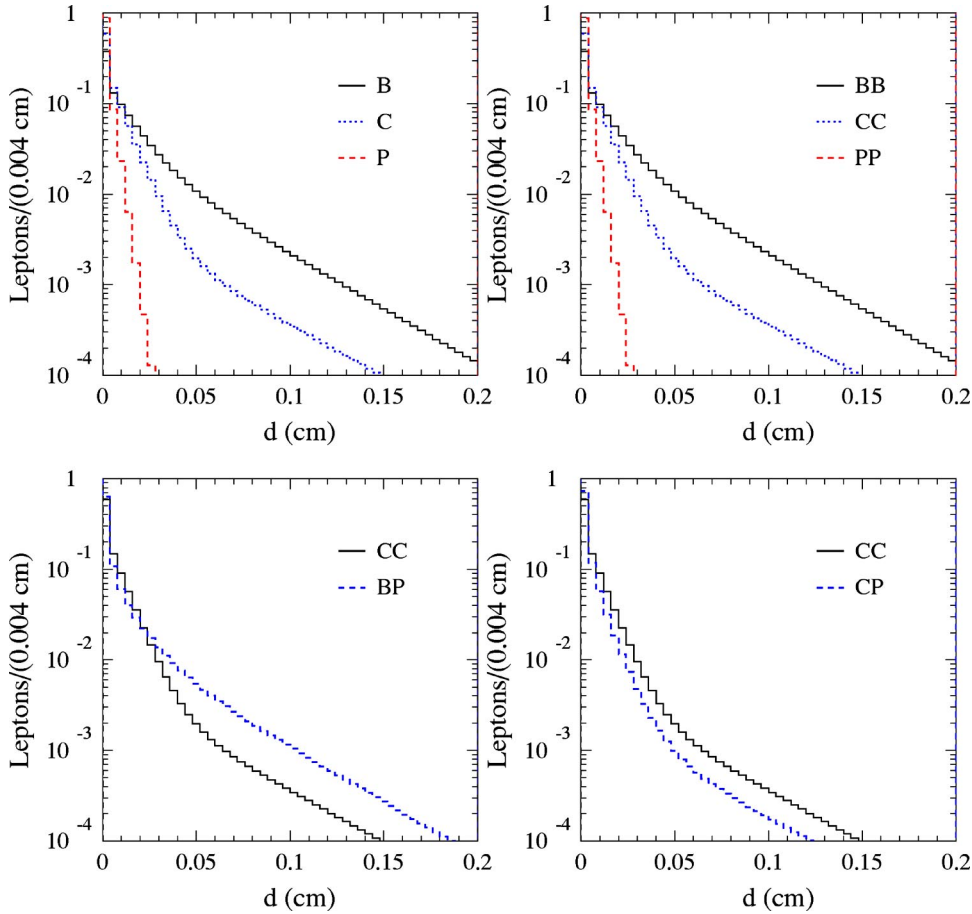


FIG. 3. Projections of the two-dimensional impact parameter distributions of the different components used to fit the dimuon data (see text). The top-left distribution shows the shapes of the prompt, b and c templates used to construct the different two-dimensional distributions used in the likelihood function. All distributions are normalized to unit area.

V. RESULT

We show the result of the fit to the data for dimuon and $e\mu$ events in subsections A and B, respectively.

A. Dimuon events

The observed two-dimensional impact parameter distributions for OS and LS dimuons are plotted in Fig. 4. We do not use dimuon events with invariant mass between 9.2 and 10.5 GeV/c^2 since OS are largely dominated by Y meson

production. There are 18420 OS dimuons and 9279 LS dimuons after the removal of 6264 OS and 1302 LS dimuons with invariant mass in the Y region.

One sees that a handful of events in Fig. 4(a) cluster along the diagonal line $d_1 = d_2$. These events are due to cosmic rays. We minimize their contribution by fitting only events with $d_1 + d_2 \leq 0.2$ cm. As shown in Sec. VII, the fit result is unaffected by the inclusion of events with $d_1 + d_2 \geq 0.2$ cm. When all the likelihood terms are used to fit the data, the best fit, as expected, returns $CC = 0 \pm 40$ LS events. However,

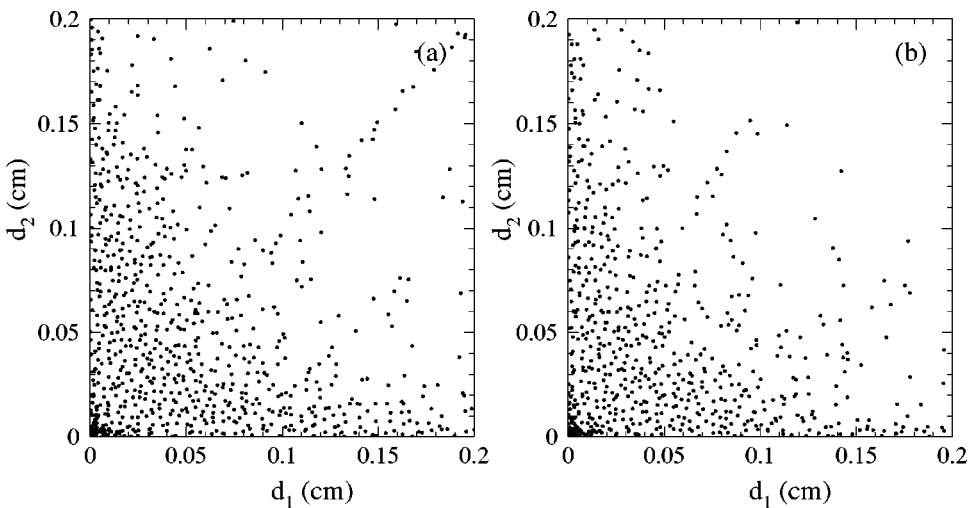


FIG. 4. Two-dimensional impact parameter distributions for (a) OS and (b) LS dimuons.

TABLE I. Number of events attributed to the different sources of dimuons by the fit to OS and LS dimuons with $d_1+d_2 \leq 0.2$ cm. The errors correspond to a 0.5 change of $-\ln L$.

Component	OS	LS
<i>BB</i>	10476 ± 223	5630 ± 132
<i>CC</i>	2469 ± 360	0
<i>PP</i>	3603 ± 161	1914 ± 87
<i>BP</i>	1566 ± 165	1555 ± 157
<i>CP</i>	0	0

while the fit finds an appreciable *BP* component, it returns $CP=0 \pm 110$ in both LS and OS events. When fitting the data with all components, the fit gets blocked when limiting the *CC*(*LS*) and *CP* parameters to positive values, and it returns reliable errors only when allowing the *CC* and *CP* terms to have also unphysical (negative) values. Since these unphysical values produce an overestimate of the size and the error of the remaining components, we fit again the data setting to zero the *CC* term in LS events and the *CP* contribution to OS and LS events.¹⁰

The fit result is shown in Table I. The parameter correlation matrix is listed in Table II. The best fit returns $-\ln L = 3076$. The probability of the $-\ln L$ value returned by the fit is determined by fitting Monte Carlo pseudoexperiments. In each experiment, we randomly generate different components with average size as determined by the fit to the data and allowing for Poisson fluctuations; the impact parameter distribution for each component is randomly generated from the corresponding templates used in the fit. We find that 40% of the fits to the pseudoexperiments return a $-\ln L$ value equal or larger than 3076. For a comparison of the data and the fit results, projections of the two-dimensional impact parameter distributions are shown in Fig. 5. Since the fit appears to underestimate the data for $d_1 \geq 0.12$ cm, we have fitted the data excluding points at impact parameters larger than 0.12 cm; this fit returns a result identical to that of the standard fit. Using Table I, one derives a ratio of LS to OS dimuons due to $b\bar{b}$ production which is $R = 0.537 \pm 0.018$.

¹⁰In Sec VII, we show that this happens in 15% of simulated pseudoexperiments due to the fact that *CC*, *BP*, and *CP* templates are quite similar. In addition, we show that the fit result does not vary when constraining the *BP* and *CP* components to be, as expected, equal within their statistical error.

B. $e\mu$ events

Figure 6 shows the observed two-dimensional impact parameter distributions for OS and LS $e\mu$ pairs. There are 7802 OS and 4331 LS $e\mu$ events.¹¹

When all the likelihood terms are used to fit the data, the best fit, as expected, returns $CC=0 \pm 80$ LS events. However, while the fit finds an appreciable *BP* component, it returns $CP=0 \pm 130$ in both LS and OS events. As in the case of dimuon events, the fit gets blocked at the lower limits when the *CC*(*LS*) and *CP* parameters are bound to be positive, and we exclude these terms in the fit likelihood. The fit result is shown in Table III and the parameter correlation matrix is listed in Table IV. The best fit returns $-\ln L = 2481$. As for dimuon events, the probability of the $-\ln L$ value returned by the fit is determined by fitting Monte Carlo pseudoexperiments. We find that 62% of the fits to the pseudoexperiments return $-\ln L$ values equal or larger than 2481. For a comparison of the data and the fit result, projections of the two-dimensional impact parameter distributions are shown in Fig. 7. Since the fit appears to underestimate the data for $d_1 \geq 0.1$ cm, we have fitted the data excluding points at impact parameters larger than 0.1 cm; this fit returns a result identical to that of the standard fit. Using Table III one derives that the ratio of LS to OS dileptons due to $b\bar{b}$ production is $R = 0.560 \pm 0.024$.

VI. AVERAGE $B^0\bar{B}^0$ MIXING PROBABILITY

The average $B^0\bar{B}^0$ mixing probability is defined as

$$\bar{\chi} = \frac{\Gamma(B^0 \rightarrow \bar{B}^0 \rightarrow l^+ X)}{\Gamma(B \rightarrow l^+ X)},$$

where the numerator includes B_d^0 and B_s^0 mesons and the denominator includes all B hadrons. In absence of mixing, the double semileptonic decay of a $B\bar{B}$ pair results in an OS lepton pair; when one of the mesons undergoes mixing a LS lepton pair is produced. The mixing probability $\bar{\chi}$ can therefore be inferred from R , the ratio of LS to OS dileptons due to $b\bar{b}$ production.

¹¹Since lepton tracks are reconstructed requiring at least two hits in the SVX detector close to the beam pipe, the number of electrons due to unidentified photon conversion is negligible (no larger than three).

TABLE II. Parameter correlation coefficients returned by the fit listed in Table I.

Component	<i>BB</i> (<i>OS</i>)	<i>CC</i> (<i>OS</i>)	<i>PP</i> (<i>OS</i>)	<i>BP</i> (<i>OS</i>)	<i>BB</i> (<i>LS</i>)	<i>PP</i> (<i>LS</i>)
<i>CC</i> (<i>OS</i>)	-0.70					
<i>PP</i> (<i>OS</i>)	0.53	-0.73				
<i>BP</i> (<i>OS</i>)	-0.03	-0.46	0.05			
<i>BB</i> (<i>LS</i>)	0.02	0.31	-0.03	-0.66		
<i>PP</i> (<i>LS</i>)	0.02	0.27	-0.03	-0.58	0.25	
<i>BP</i> (<i>LS</i>)	-0.03	-0.44	0.05	0.94	-0.71	-0.62

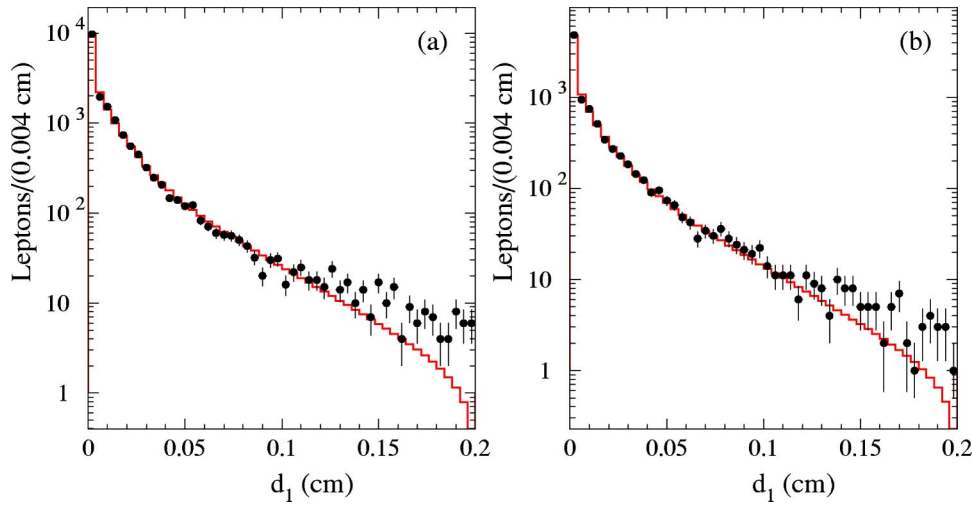


FIG. 5. The projection of the impact parameter distribution of (a) OS and (b) LS dimuons onto one of the two axis is compared to the fit.

The sequential decays of b hadrons also contribute to R . The fraction of leptons from sequential decays f_l is evaluated using the simulation. Using simulated dimuon events, we find $f_\mu = 0.123$ with a 12% uncertainty.¹² As for the study of Ref. [4], the uncertainty on f_μ comes from the uncertainty of the relative branching ratios of b and c semileptonic decays ($\pm 11\%$) and the uncertainty of the detector acceptance for sequential leptons with respect to that for leptons from direct decays ($\pm 6\%$). Using the $e\mu$ simulation, we derive $f_e = 0.060$ and $f_\mu = 0.142$ with a $\pm 12\%$ systematic uncertainty.

The ratio R is related to the time-integrated mixing probability in the following way:

$$R = \frac{f[\bar{\chi}^2 + (1 - \bar{\chi})^2] + 2\bar{\chi}(1 - \bar{\chi})(1 - f)}{(1 - f)[\bar{\chi}^2 + (1 - \bar{\chi})^2] + 2\bar{\chi}(1 - \bar{\chi})f},$$

where $f = 2f_\mu(1 - f_\mu) = 0.2157 \pm 0.0226$ (syst) for dimuon events and $f = f_e + f_\mu - 2f_e f_\mu = 0.1850 \pm 0.0204$ (syst) for

$e\mu$ events. Systematic errors due to other sources are negligible with respect to that arising from the f uncertainty, and are neglected (see Sec. VII).

From the observed values of R , we derive the following mixing probabilities:

$$\bar{\chi} = 0.136 \pm 0.009 \text{ (stat)} \pm 0.014 \text{ (syst)} \text{ for dimuon events,}$$

$$\bar{\chi} = 0.165 \pm 0.011 \text{ (stat)} \pm 0.011 \text{ (syst)} \text{ for } e\mu \text{ events.}$$

Since we use events containing two and only two leptons, the results from the dimuon and $e\mu$ data sets are statistically independent. Therefore, we combine the two results and derive an average mixing probability $\bar{\chi} = 0.152 \pm 0.007$ (stat) ± 0.011 (syst).¹³

This value of the mixing probability agrees with all previous results from $p\bar{p}$ colliders:

¹³The systematic error is evaluated by changing simultaneously f_e and f_μ by their 12% uncertainty. The systematic error quoted in Ref. [4] (± 0.016) is larger to account for the fact that the BP and CC terms are not fitted independently.

¹²Technically this fraction accounts also for the 0.4% fraction of events which contain more than two hadrons with heavy flavor.

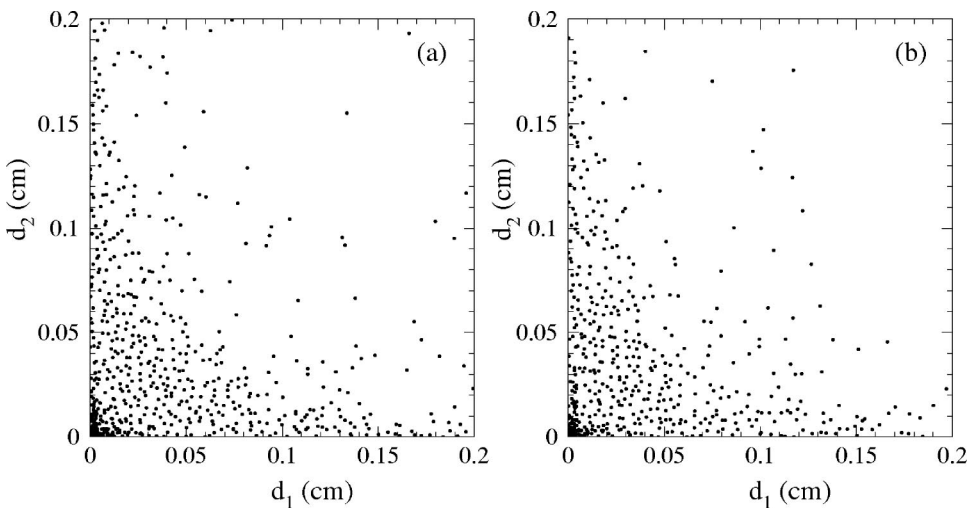


FIG. 6. Two-dimensional impact parameter distributions for (a) OS and (b) LS $e\mu$ events.

TABLE III. Number of events attributed to the different sources by the fit to OS and LS $e\mu$ pairs. The errors correspond to a 0.5 change of $-\ln L$.

Component	OS	LS
BB	5099 ± 138	2852 ± 90
CC	1126 ± 162	0
PP	906 ± 60	875 ± 52
BP	536 ± 107	529 ± 102
CP	0	0

$$\bar{\chi} = 0.157 \pm 0.020 \text{ (stat)} \pm 0.032 \text{ (syst)} \text{ (UA1 [12])},$$

$$\bar{\chi} = 0.176 \pm 0.031 \text{ (stat+syst)} \\ \pm 0.032 \text{ (model)} \text{ (CDF [13])},$$

$$\bar{\chi} = 0.131 \pm 0.020 \text{ (stat)} \pm 0.016 \text{ (syst)} \text{ (CDF [4])}$$

but is significantly larger than the world average $\bar{\chi} = 0.118 \pm 0.005$ [3], which is dominated by the LEP measurements at the Z pole.¹⁴ Since our result is statistically very different from the world average, we have investigated the error behavior beyond one σ . For an 8 unit increase of the $-\ln L$ value (4σ uncertainty), the errors of the $BB(OS)$ and $BB(LS)$ terms returned by the fit increase by a factor of four, and we derive a 4σ statistical error of 0.029 for the combined value of $\bar{\chi}$.

VII. CROSS CHECKS OF THE RESULT AND STUDY OF ADDITIONAL SYSTEMATIC EFFECTS

In this section, we first perform several cross checks of the $\bar{\chi}$ result, and then investigate its sensitivity to the modeling of the production and weak decay of heavy quarks. In subsection A we verify that the ratio of the number of lepton pairs due to $c\bar{c}$ production to that due to $b\bar{b}$ production returned by the various fits is consistent with the theoretical expectation. Subsection B compares our result to the previous CDF measurement, which used a subset of the data available for this analysis. Subsection B also verifies that the

¹⁴The world average assumes that the fractions f_d and f_s at the Tevatron are equal to those at the Z pole.

$\bar{\chi}$ result is not affected by the small cosmic ray background present in the dimuon data sample. Subsection C shows that the $\bar{\chi}$ result is not affected by the fact that we have excluded the CP component in the fit likelihood. Subsections D, E, and F explore the dependence of our result on the mixture of the different b and c hadrons, on the ratio of $b\bar{b}$ to $c\bar{c}$ production cross section, and on the transverse momentum distribution of hadrons with heavy flavor predicted by the QCD simulation. In analogous measurements, these effects are usually not considered since they are hard to quantify and to implement consistently into the QCD generator. We investigate them either by changing the heavy flavor composition of the data with proper kinematical selections, or with reasonable modifications of the simulation prediction. Finally, subsections G and H verify the templates used to separate the contribution of semileptonic decays of heavy flavor from that of leptons due to misidentified hadrons or prompt sources as the Drell-Yan process. We show that all above effects change our result by a very small fraction of the quoted statistical and systematic errors. We report changes in R when the sequential fraction f_l is not affected by the particular study, and also changes in $\bar{\chi}$ when f_l is affected; a summary of the different results is presented in subsection I.

A. Ratio of the $c\bar{c}$ to $b\bar{b}$ production

The difference between the $\bar{\chi}$ measurements at the Tevatron and LEP may not require an explanation in terms of new physics; however, if we entertain the hypothesis [1] that the enhancement of the $b\bar{b}$ cross section at the Tevatron with respect to the NLO prediction may be caused by pair production of light gluinos decaying to a bottom quark and a bottom squark, which in turn produces an apparent increase of $\bar{\chi}$ with respect to LEP, then the ratio of the $c\bar{c}$ to $b\bar{b}$ cross sections should be approximately a factor of two smaller than what is predicted by the standard model. Therefore, it is of interest to compare the ratio of the numbers of leptons due to $c\bar{c}$ and $b\bar{b}$ production in the data and the simulation.

The dimuon fit in Table I returns a ratio $CC/BB = 0.15 \pm 0.02$ (stat). In the simulation, this ratio is 0.18 ± 0.02 (stat).

The fit to $e\mu$ data in Table III returns a ratio $CC/BB = 0.14 \pm 0.02$ (stat). In the simulation, the ratio is 0.12 with a negligible statistical error.

As shown in Ref. [14], which studies events with jets corresponding to partons with transverse momentum larger

TABLE IV. Parameter correlation coefficient returned by the fit listed in Table III.

Component	$BB(OS)$	$CC(OS)$	$PP(OS)$	$BP(OS)$	$BB(LS)$	$PP(LS)$
$CC(OS)$	-0.63					
$PP(OS)$	0.38	-0.37				
$BP(OS)$	-0.23	-0.33	-0.43			
$BB(LS)$	0.12	0.29	0.18	-0.67		
$PP(LS)$	0.31	-0.14	0.76	-0.56	0.23	
$BP(LS)$	-0.23	-0.29	-0.45	0.95	-0.70	-0.59

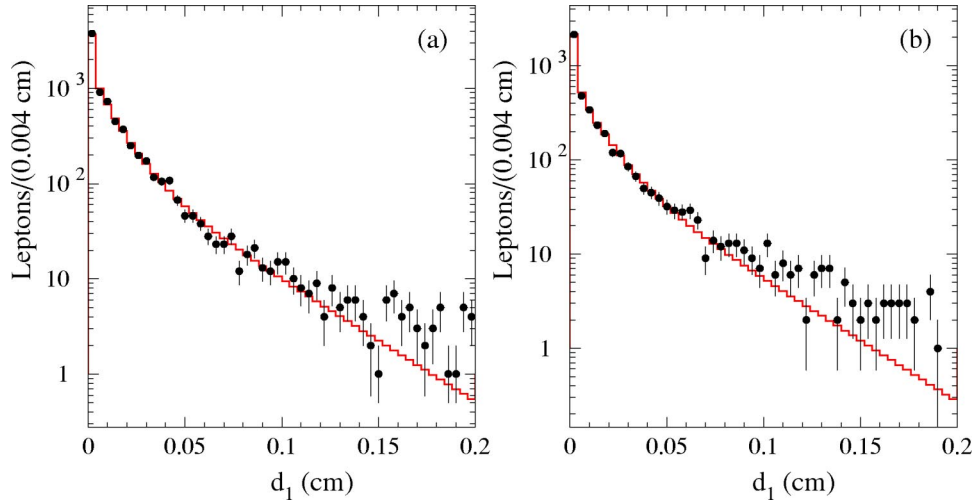


FIG. 7. The projection of the impact parameter distribution of (a) OS and (b) LS $e\mu$ pairs onto one of the two axis is compared to the fit.

than 20 GeV/c, the HERWIG generator predicts heavy flavor cross sections which are approximately a factor of two larger than the NLO calculation [15] and models correctly the $c\bar{c}$ and $b\bar{b}$ cross section observed at the Tevatron. However, muons in the present analysis correspond to partons with $p_T \geq 6.5$ GeV/c (electrons to partons with $p_T \geq 9$ GeV/c). *A priori*, there is no guarantee that HERWIG still does a good job in predicting the ratio CC/BB also in this data set which corresponds to a hard scattering with smaller transverse momenta (the inclusive $b\bar{b}$ and $c\bar{c}$ cross sections are approximately a factor of 40 larger in this data set than in the jet data studied in Ref. [14]). We cross check the ratio of the $c\bar{c}$ to $b\bar{b}$ parton-level cross sections evaluated with HERWIG with two different NLO Monte Carlo calculations. In HERWIG, the ratio of the $c\bar{c}$ to $b\bar{b}$ cross sections for producing both heavy quarks with $|\eta| \leq 1$ and transverse momentum large enough to produce an electron with $E_T \geq 5$ GeV and a muon with $p_T \geq 3$ GeV/c is 1.37. In the MNR calculation [15], this ratio is found to be 1.39, while the CASCADE Monte Carlo generator [16] predicts a value of 1.35 [17]. We conclude that the ratio of dileptons due to $c\bar{c}$ production to that due to $b\bar{b}$ production at the Tevatron is consistent with the prediction of the presently available Monte Carlo generators.

B. Cosmic ray background in dimuon events and comparison with the previous CDF result

The previous CDF measurement of $\bar{\chi}$ [4] uses a subset (17.4 pb⁻¹) of the dimuon sample (105 pb⁻¹) collected by CDF and used in the present analysis. There are minor differences in the data selection. In the present analysis we exclude dimuons with impact parameters $d_1 + d_2 \geq 0.2$ cm to reduce the impact of the cosmic ray background, and we exclude the Y invariant mass region which has a negligible fraction of heavy flavor contribution.

To study our sensitivity to the cosmic ray background we have performed a fit to the data which includes dimuons with $d_1 + d_2 \geq 0.2$ cm. This fit returns a ratio $R = 0.533 \pm 0.018$ (the standard fit yields $R = 0.537 \pm 0.018$). We conclude that

the small cosmic ray background does not affect the fit result.

In order to compare with the result in Ref. [4] we fit the data including the Y mass region. Because of the slightly different selection, the total number of events in the present analysis, 35265, is 24% larger than the number of events selected in Ref. [4] (4750 events) multiplied by the ratio of the relative luminosities. The fit which includes this mass region is shown in Table V. The fit returns a total of 18737 ± 275 dimuon events due to $b\bar{b}$ production. Consistently, this number is 25% larger than the number of dimuon events attributed in Ref. [4] to $b\bar{b}$ production (2471 ± 104 events) multiplied by the ratio of the relative luminosities. This fit that includes the Y mass region yields $R = 0.535 \pm 0.017$ (stat), which compares well to the result of our standard fit and the value $R = 0.502 \pm 0.041$ (stat) in Ref. [4].

C. Effect of neglecting the CP component in the likelihood function

In order to estimate correctly the uncertainties of the $b\bar{b}$ and $c\bar{c}$ contributions returned by the fit, we had to set to zero the CP component, which is expected to be of the same size of the BP component.⁹ We have performed a number of pseudoexperiments of approximately the same size and composition as the data. In each pseudoexperiment, the impact parameters of the dileptons contributed by a given component are extracted from the corresponding two-dimensional

TABLE V. Number of events attributed to the different sources of dimuons by the fit to OS and LS dimuons including the invariant mass region between 9.2 and 10.5 GeV/c².

Component	OS	LS
BB	12202 ± 237	6535 ± 139
CC	2849 ± 388	0
PP	7601 ± 189	2173 ± 94
BP	1662 ± 175	1658 ± 167
CP	0	0

TABLE VI. Number of generated and fitted events in 125 pseudoexperiments. We list the average and the rms spread of the values returned by the fits.

Component	Generated	Fitted
<i>BB</i>	8000	7998 ± 247
<i>CC</i>	4000	3991 ± 544
<i>PP</i>	4000	3999 ± 348
<i>BP</i>	1200	1204 ± 505
<i>CP</i>	1200	1196 ± 812

template used to fit the data. Each pseudoexperiment has been fitted as the data, and the result of 125 pseudoexperiments is shown in Table VI. In 15% of the pseudoexperiments, the *CP* value returned by the fit is so close to zero that the fit gets blocked at the lower limit; as for the data, the *CP* term has to be ignored in the likelihood in order to estimate correctly the uncertainty of the *BB* term.

We have further investigated the sensitivity of the *R* result to the value of the *CP* component returned by the fit by constraining it to be equal to the *BP* contribution within the statistical error. The fit results are shown in Table VII for dimuon events and in Table VIII for $e\mu$ events. These fits return $R=0.533 \pm 0.016$ (the standard fit returns $R=0.537 \pm 0.018$) for dimuon events and $R=0.559 \pm 0.023$ (the standard fit returns $R=0.560 \pm 0.024$) for $e\mu$ events.

D. Sensitivity to the *b* and *c* lifetime

The impact parameter distribution of leptons from *b* and *c* decays has some dependence on the lifetime uncertainty. We have varied the average *b*-hadron lifetime in the simulation by $\pm 10\%$ and refit the data with the resulting templates in order to investigate which effect might have the possibility that the relative fractions of different *b* hadrons in the simulation are grossly different from the data. The fractions of the *BB* components, which are returned by the fit, change by approximately $\pm 9\%$ for both OS and LS dileptons; however, the ratio *R* changes by less than 0.2%.

Since $c\bar{c}$ events contribute only to OS events, we have studied the sensitivity of the fit to the impact parameter template for *c* semileptonic decays. We have constructed impact parameter templates by varying in the simulation the relative

TABLE VII. Number of events attributed to the different sources of dimuons by the fit to OS and LS dimuons with $d_1 + d_2 \leq 0.2$ cm. The errors correspond to a 0.5 change of $-\ln L$.

Component	OS	LS
<i>BB</i>	10691 ± 232	5695 ± 134
<i>CC</i>	2203 ± 404	0
<i>PP</i>	3328 ± 166	1536 ± 122
<i>BP</i>	1009 ± 130	1001 ± 126
<i>CP</i>	878 ± 122	869 ± 117

TABLE VIII. Number of events attributed to the different sources by the fit to OS and LS $e\mu$ events. The errors correspond to a 0.5 change of $-\ln L$.

Component	OS	LS
<i>BB</i>	5171 ± 134	2892 ± 92
<i>CC</i>	1083 ± 162	0
<i>PP</i>	798 ± 70	767 ± 64
<i>BP</i>	312 ± 63	308 ± 60
<i>CP</i>	300 ± 61	293 ± 58

ratio of D^\pm to D^0 mesons by $\pm 30\%$.¹⁵ The *CC* component in OS dileptons returned by the fit changes by approximately $\pm 10\%$. In the fit, this change is mostly compensated by the *BP* component, and the *BB* contribution to OS dilepton changes by less than $\pm 0.1\%$.

E. Sensitivity to the $c\bar{c}$ contribution

The $c\bar{c}$ production contributes only OS dileptons. The value of *R* returned by the fit can be affected by a poor modeling of this contribution. We investigate this possibility by analyzing a data sample with a smaller fraction of $c\bar{c}$ contribution. According to the HERWIG generator program, and also to the MNR Monte Carlo program [15], the ratio of the $c\bar{c}$ to $b\bar{b}$ cross sections for producing both heavy flavor partons with $|\eta| \leq 1$ and transverse momenta larger than 9 GeV/*c* is 1 while in the simulation of the standard $e\mu$ data set is 1.37.

This kinematical situation is modeled by selecting muons, as well as electrons, with $p_T \geq 5$ GeV/*c*. We derive from the simulation of this data set new impact parameter templates for *b*- and *c*-hadron decays. The fit result is shown in Table IX. The fit yields $R=0.524 \pm 0.034$. In this case, the fractions of sequential decays are $f_e=0.060$, $f_\mu=0.092$, and $f=0.1410 \pm 0.0158$ (syst). It follows that $\bar{\chi}=0.170 \pm 0.015$ (stat) ± 0.007 (syst), in agreement with the result of the standard fit $\bar{\chi}=0.165 \pm 0.011$ (stat) ± 0.011 (syst).

F. Sensitivity to the modeling of the kinematics

Because we select leptons above a certain p_T threshold, the impact parameter templates for leptons from semileptonic decays of heavy flavors have some dependence on the modeling of the p_T distribution of the parent hadron with heavy flavor.¹⁶ The modeling of the p_T distribution of the parent hadron with heavy flavor can be affected by a wrong estimate of the relative contribution of processes of order α_s^2 and α_s^3 , or by an incorrect modeling of the hadronization of

¹⁵The lifetime is $c\tau=315 \mu\text{m}$ for the D^\pm meson and $c\tau=123 \mu\text{m}$ for the D^0 meson.

¹⁶In the extreme case of a lepton with p_T close to the 5 GeV/*c* threshold, parent hadrons with a 5 GeV transverse energy produce leptons with zero impact parameter.

TABLE IX. Number of events attributed to the different sources by the fit to OS and LS $e\mu$ events in which both leptons have $p_T \geq 5$ GeV/ c . The errors correspond to a 0.5 change of $-\ln L$.

Component	OS	LS
BB	2113 ± 86	1107 ± 57
CC	421 ± 98	0
PP	265 ± 36	249 ± 31
BP	163 ± 68	159 ± 65
CP	0	0

heavy quarks.¹⁷ In the next two subsections, we investigate the sensitivity of our result to these effects.

1. Dileptons with $\delta\phi \geq 2.4$

According to the simulation, the fractional contribution of $b\bar{b}$ and $c\bar{c}$ direct production (LO term) increases with increasing $\delta\phi$, the azimuthal opening angle between the two leptons. Using dileptons with $\delta\phi \geq 2.4$ rad, the number of simulated events due to $b\bar{b}$ and $c\bar{c}$ production is reduced by 64 and 66%, respectively. At the same time, the fraction of direct production in $b\bar{b}$ events increases from 71 to 84% and the fraction of direct production in $c\bar{c}$ events increases from 66 to 76%.

Using this selection, the data consist of 4872 OS and 2745 LS dileptons. The result of the fit to these events using standard templates is shown in Table X. We derive $R = 0.576 \pm 0.032$, in good agreement with the standard fit result $R = 0.560 \pm 0.024$.

2. Dependence on the p_T spectrum of the parent hadron with heavy flavor

As shown by Fig. 21 of Ref. [18] and Figs. 7 and 8 of Ref. [14], our simulation models quite well the hadronization of b and c quarks with transverse energy larger than 20 GeV. As shown in Fig. 8, the simulation also models correctly the lepton transverse momentum distributions in the $e\mu$ data. Because the lepton distribution depends on the p_T distribution of the parent parton and its fragmentation function, we use a comparison between data and simulation to evaluate their global uncertainty. A fit of the lepton p_T spectra with the simulated shapes weighted with the function p_T^α , where α is a free fit parameter, returns $\alpha = 0.003 \pm 0.023$. In the simulation, such changes of lepton p_T distributions can be modeled by reweighting the p_T distribution of the parent parton with the function $p_T^{\pm\beta=0.5}$. Fits to the $e\mu$ data using templates constructed with these modified simulations return

¹⁷In the simulation partons arising from α_s^2 diagrams are slightly stiffer than those contributed by α_s^3 diagrams.

TABLE X. Number of events attributed to the different sources by the fit to OS and LS $e\mu$ events with $\delta\phi \geq 2.4$. The errors correspond to a 0.5 change of $-\ln L$.

Component	OS	LS
BB	3255 ± 110	1874 ± 75
CC	688 ± 129	0
PP	534 ± 47	513 ± 41
BP	314 ± 88	310 ± 84
CP	0	0

$R = 0.557 \pm 0.024$ for $\beta = 0.05$ and $R = 0.559 \pm 0.024$ for $\beta = -0.05$ (the result of the standard fit is 0.560 ± 0.023).

G. Dependence on the modeling of the impact parameter distributions

For tracks in a jet, the impact parameter resolution in the data is slightly larger than in the parametrized QFL detector simulation which has in input the SVX-hit resolution of the data [8]. This is believed to be due to the probability of reconstructing a track with spurious SVX hits, which in the data is larger than in the simulation because the SVX occupancy in the data is also larger. In JET 20 data,¹⁸ the transverse energy deposited by charged tracks in a cone of radius 0.2 in the η - ϕ space around the axis of a lepton contained in a jet is ≈ 18 GeV. For the events used in this analysis, the transverse energy deposited by charged tracks in a cone of radius 0.2 around each lepton is ≈ 0.8 GeV; in this case, the transverse momentum distribution of all charged tracks in the dilepton events, plotted in Fig. 8(c), is also well modeled by the simulation.

To further investigate the sensitivity to spurious SVX hits, we have repeated our study by using only leptons with 4 SVX hits; we also require that at least two of the hits are not shared with other tracks. We also make use of new templates for prompt leptons, and leptons from b - and c -hadron decays constructed using this track selection.

With this selection, the dimuon data consist of 9822 OS and 4785 SS pairs. Table XI lists the result of the fit to dimuon events passing this selection. The fit yields $R = 0.548 \pm 0.025$, in good agreement with the result of the standard fit $R = 0.537 \pm 0.018$.

The $e\mu$ data consist of 4465 OS and 2355 SS pairs with 4 SVX hits. Table XII lists the fit result. The fit yields $R = 0.559 \pm 0.029$, in good agreement with the result of the standard fit $R = 0.560 \pm 0.024$. For a comparison of the data and the fit results, projections of the two-dimensional impact parameter distributions are shown in Fig. 9. The combined result yields an average mixing parameter $\bar{\chi} = 0.154 \pm 0.009$ (stat) ± 0.011 (syst), to be compared to the standard fit result $\bar{\chi} = 0.152 \pm 0.007$ (stat) ± 0.011 (syst).

¹⁸Events collected with a trigger that requires at least one jet with $E_T \geq 20$ GeV.

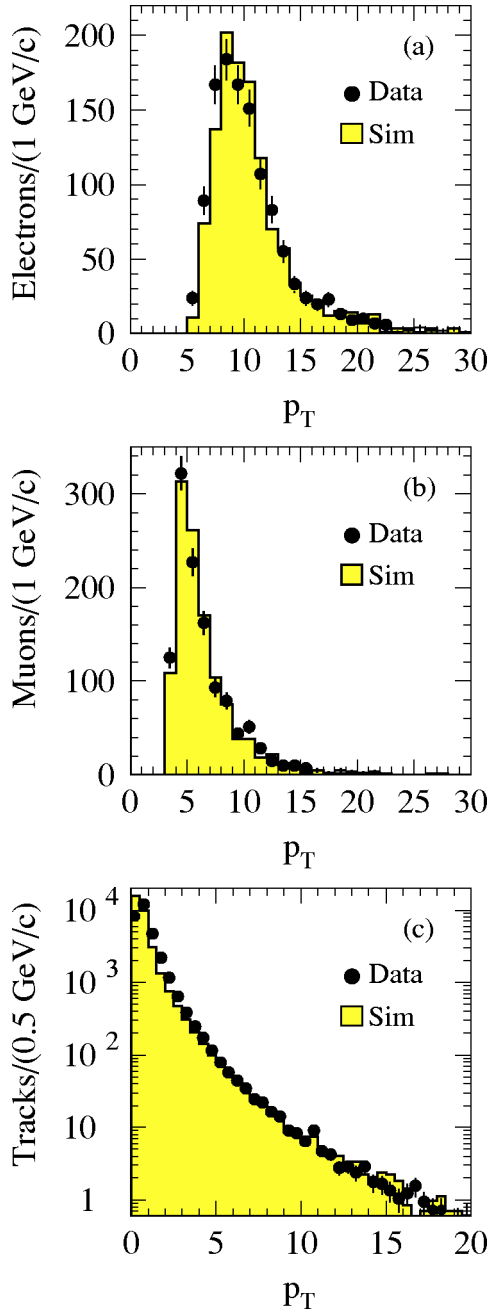


FIG. 8. Comparison of the transverse momentum distributions of electrons (a) and muons (b) in the data and in the heavy flavor simulation. The bottom plot (c) shows the transverse momentum distribution of all other tracks in $e\mu$ events. Data and simulation are normalized to the same number of events.

H. Leptons faked by tracks from hadronic decays of hadrons with heavy flavor

In the standard fit to the data, we have approximated the impact parameter distribution of fake leptons with that of leptons from prompt sources. The fits return a BP component which is 15% (dimuon events) and 10% ($e\mu$ events) of the BB component. According to the simulation, only 7.5% of the events due to the BP component contain a second hadron with heavy flavor which decays hadronically; in these events,

TABLE XI. Number of events attributed to the different sources by the fit to OS and LS dimuons with 4 SVX hits and $d_1+d_2 \leq 0.2$ cm. The errors correspond to a 0.5 change of $-\ln L$.

Component	OS	LS
BB	4990 ± 150	2735 ± 90
CC	1818 ± 245	0
PP	2237 ± 112	1289 ± 63
BP	740 ± 110	743 ± 106
CP	0	0

less than 50% of the tracks, which are fake-lepton candidates, arise from the decay of the heavy flavored hadron; in addition, 80% of the lepton faked by tracks from hadronic decays of heavy flavors carry a charge with the same sign of that of the parent heavy flavor quark. Therefore, one estimates that the effect of this approximation on R is of the order of 10^{-3} .¹⁹

We cross check our conclusion by modeling fake leptons with new templates, called F (instead of P), derived in a sample with a comparable contamination of hadrons with heavy flavor. This sample consists of events containing a jet with $E_T \geq 20$ GeV. As shown by the study in Ref. [8], JET 20 data contain a 9.5% fraction of heavy flavor. After removing events in which jets contain a soft lepton (SLT tag) or a displaced secondary vertex (SECVTX tag), the contamination of heavy flavor is 7.1% (comparable to the fraction of heavy flavor with hadronic decay contributing to the BF and CF components). The new template is constructed by using all tracks with $p_T \geq 3$ GeV/c and pointing to the CMUP fiducial volume. Figure 10 compares the new template to the one derived using prompt muons.

Tables XIII and XIV list the results of the fits to dilepton events with 4 SVX hits when using templates which account for the heavy flavor contribution to fake leptons. The fits return $R = 0.570 \pm 0.027$ for dimuon events and $R = 0.562 \pm 0.034$ for $e\mu$ events. The combined result yields an average mixing probability $\bar{\chi} = 0.159 \pm 0.010$ (stat)

¹⁹This is supported by the fact that the CC component in LS dileptons, which can only be contributed by leptons faked by tracks from hadronic decays of charmed hadrons, is found negligible by our fit with a 1σ upper limit of 1.6% of the CC contribution to OS dileptons.

TABLE XII. Number of events attributed to the different sources by the fit to OS and LS $e\mu$ events with 4 SVX hits. The errors correspond to a 0.5 change of $-\ln L$.

Component	OS	LS
BB	2768 ± 99	1547 ± 66
CC	831 ± 121	0
PP	575 ± 44	552 ± 37
BP	266 ± 76	264 ± 73
CP	0	0

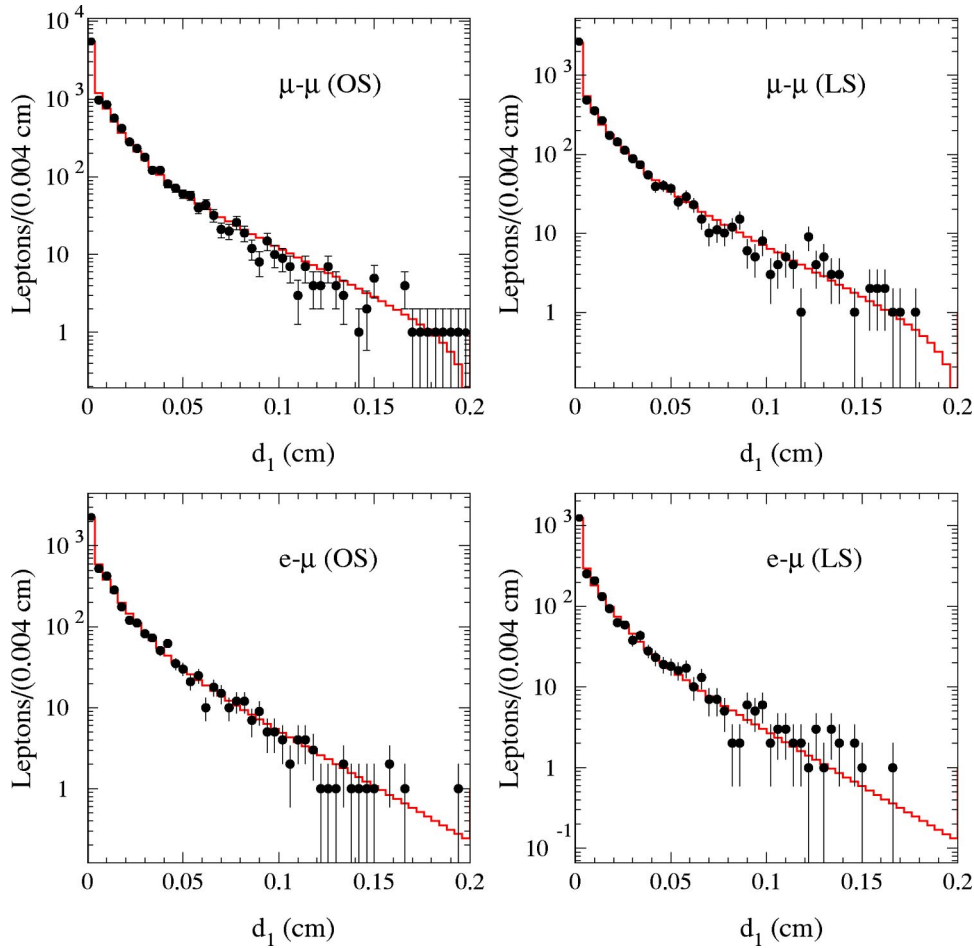


FIG. 9. The projection of the impact parameter distributions in the data is compared to the fit results.

± 0.011 (syst) to be compared to the standard fit result $\bar{\chi} = 0.154 \pm 0.009$ (stat) ± 0.011 (syst).

I. Summary of the cross checks

Table XV lists the $\bar{\chi}$ values resulting from the different cross checks presented in this section. All $\bar{\chi}$ measurements are consistent with the main result presented in Sec. VI.

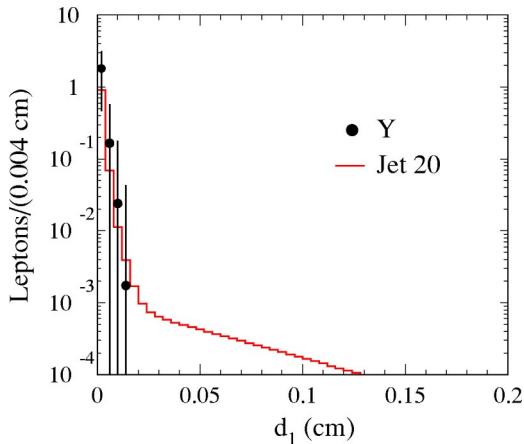


FIG. 10. Comparison of the impact parameter distributions of lepton candidate tracks in JET 20 data and of leptons coming from $Y(1S)$ decays.

VIII. CONCLUSIONS

Using samples of $\mu\mu$ and $e\mu$ pairs collected with the CDF experiment during the 1992–1995 run of the Tevatron collider, we have performed a high precision measurement of $\bar{\chi}$, the time integrated mixing probability of b -flavored hadrons produced at the Tevatron. Our measurement, $\bar{\chi} = 0.152 \pm 0.007$ (stat) ± 0.011 (syst), confirms the trend of all previous results from $p\bar{p}$ colliders, and is significantly larger than the world average $\bar{\chi} = 0.118 \pm 0.005$, which is dominated by the LEP measurements at the Z pole.

TABLE XIII. Number of events attributed to the different sources of dimuons by the fit to OS and LS dimuons with 4 SVX hits and $d_1 + d_2 \leq 0.2$ cm. Fake leptons for the BF and CF components are modeled with a template derived in JET 20 data.

Component	OS	LS
BB	4781 ± 150	2723 ± 90
CC	2207 ± 222	0
PP	2018 ± 111	1251 ± 64
BF	787 ± 108	796 ± 104
CF	0	0

TABLE XIV. Number of events attributed to the different sources of dimuons by the fit to OS and LS $e\mu$ with 4 SVX hits. Fake leptons for the BF and CF components are modeled with a template derived in JET 20 data.

Component	OS	LS
BB	2743 ± 103	1541 ± 68
CC	857 ± 118	0
PP	586 ± 45	566 ± 38
BF	257 ± 76	256 ± 73
CF	0	0

ACKNOWLEDGMENTS

We thank the Fermilab staff and the technical staff of the participating Institutions for their contributions. This work was supported by the U.S. Department of Energy and National Science Foundation, the Istituto Nazionale di Fisica Nucleare, the Ministry of Education, Culture, Sports, Science and Technology of Japan, the Natural Science and Engineering Research Council of Canada, the National Science Coun-

TABLE XV. Summary of the cross checks presented in Sec. VII. The $\bar{\chi}$ error is statistical only.

Data set	Fit type	$\bar{\chi}$
$\mu\mu + e\mu$	standard	0.152 ± 0.007
$\mu\mu + e\mu$	$BP = CP$ (Sec. VII C)	0.151 ± 0.007
$\mu\mu + e\mu$	4 SVX hits (Sec. VII G)	0.154 ± 0.009
$\mu\mu + e\mu$	4 SVX hits, JET 20 fakes (Sec. VII H)	0.159 ± 0.010
$e\mu$	standard	0.165 ± 0.011
$e\mu$	$\Delta\phi \geq 2.4$ rad (Sec. VII F 1)	0.173 ± 0.015
$e\mu$	$p_T^{\text{lepton}} \geq 5$ GeV/c (Sec. VII E)	0.170 ± 0.015
$e\mu$	$\beta = +0.05$ (Sec. VII F 2)	0.164 ± 0.011
$e\mu$	$\beta = -0.05$ (Sec. VII F 2)	0.165 ± 0.011

cil of the Republic of China, the Swiss National Science Foundation, the A.P. Sloan Foundation, the Bundesministerium für Bildung und Forschung, the Korea Science and Engineering Foundation (KoSEF), the Korea Research Foundation, and the Comision Interministerial de Ciencia y Tecnologia, Spain.

- [1] E. Berger *et al.*, Phys. Rev. Lett. **86**, 4231 (2001).
[2] Z. Luo *et al.*, Phys. Lett. B **569**, 194 (2003).
[3] Particle Data Group, K. Hagiwara *et al.*, Phys. Rev. D **66**, 010001 (2002).
[4] F. Abe *et al.*, Phys. Rev. D **55**, 2546 (1997).
[5] T. Affolder *et al.*, Phys. Rev. D **60**, 112004 (1999); F. Abe *et al.*, *ibid.* **60**, 072003 (1999); **60**, 051101 (1999); Phys. Rev. Lett. **80**, 2057 (1998).
[6] F. Abe *et al.*, Nucl. Instrum. Methods Phys. Res. A **271**, 387 (1988).
[7] D. Amidei *et al.*, Nucl. Instrum. Methods Phys. Res. A **350**, 73 (1994).
[8] T. Affolder *et al.*, Phys. Rev. D **64**, 032002 (2001).
[9] G. Marchesini and B.R. Webber, Nucl. Phys. **B310**, 461 (1988); G. Marchesini *et al.*, Comput. Phys. Commun. **67**, 465 (1992).
[10] Version 9_1 of the CLEO simulation; P. Avery, K. Read, and G. Trahern, Cornell Internal Note CSN-212, 25, 1985.
[11] B. Abbot *et al.*, Phys. Lett. B **487**, 264 (2000).
[12] C. Albajar *et al.*, Z. Phys. C **61**, 41 (1994).
[13] F. Abe *et al.*, Phys. Rev. Lett. **67**, 3351 (1991).
[14] D. Acosta *et al.*, hep-ex/0311051.
[15] M. Mangano *et al.*, Nucl. Phys. **B373**, 295 (1992). The FORTRAN code is available from the authors.
[16] H. Jung, J. Phys. G **28**, 971 (2002); Eur. Phys. J. C **19**, 351 (2001).
[17] H. Jung (private communication).
[18] D. Acosta *et al.*, Phys. Rev. D **65**, 052007 (2002).